Creating Magnetic Resonance Images

Ernst Binz
Lehrstuhl für Mathematik I
Universität Mannheim
D-68159 Mannheim
Germany
email: binz@math.uni-mannheim.de

Walter Schempp
Lehrstuhl für Mathematik I
Universität Siegen
D-57068 Siegen
Germany
email: schempp@mathematik.uni-siegen.de

Abstract
The soft tissue contrast provided by magnetic resonance imaging frequently makes it the modality of choice in diagnostic imaging. The paper describes the imaging modality of magnetic resonance tomography in terms of harmonic analysis on the Heisenberg Lie group.

Keywords: Quantum information processing, clinical magnetic resonance imaging, single-section acquisitions, multisection acquisition, volume acquisition

1 Introduction

The imaging modality of magnetic resonance tomography is based on the phenomenon of nuclear magnetic resonance, that is, the resonance of atomic nuclei. Due to the tremendous contributions of clinical magnetic resonance imaging in the diagnostic evaluation of patients and its superb ability to define the relevant anatomy and pathology, the study of magnetic resonance tomography has grown enormously in the past ten years. The progress in these studies is of theoretical as well as practical nature. All current magnetic resonance imaging techniques in routine clinical use are based on receiving and processing magnetic resonance signals from protons. The molecular environment where these protons are located has a profound effect on the nature of the signals created, and thus give rise to the remarkable power

and versatility of clinical magnetic resonance imaging and magnetic resonance spectroscopy ([7]).

The imaging modality of magnetic resonance provides a minimal model of quantum information transmission. The purpose of this paper is to develop the technique of multisection acquisitions on the basis of the Hopf fibration approach to clinical magnetic resonance tomography. It is based on the fact that the three–dimensional Heisenberg nilpotent Lie group G can be embedded into the loop group Loop($\mathbf{T}$) of the one–dimensional compact torus group $\mathbf{T} = \{\lambda \in \mathbf{C} || \lambda| = 1\}$. The coadjoint orbit picture of the unitary dual $\hat{G}$ of the Heisenberg group G ([5]) gives rise to the technique of interleaved spin excitations of imaging a stack of sections using multisection acquisition of proton responses. After each section has been excited once, all sections are excited a second time, using a different phase–encoding gradient. The read–out procedure is based on the symplectic Fourier transforms associated to the planar coadjoint orbits of G.

It is assumed that the reader is familiar with the basic principles of clinical magnetic resonance tomography. The details of the modality can be found in [3]. The mathematical analysis of clinical magnetic tomography based on the coadjoint orbit picture of the unitary dual $\hat{G}$ of the Heisenberg group G is in the monograph [6].

2 The sandwich configuration

The Hopf fibration $\mathbf{S}_1 \longrightarrow \mathbf{S}_3 \longrightarrow \mathbf{S}_2$ is based on the sandwich configuration of $\mathbf{R}^3$. The compact Lie group $\mathbf{T} = \mathbf{R}/\mathbf{Z}$ which is diffeomorphic to the circle

$$\mathbf{S}_1 = \{\lambda \in \mathbf{C} || \lambda| = 1\}$$

acts smoothly on the three–sphere

$$\mathbf{S}_3 = \{w = (w_0, w_1) \in \mathbf{C}^2 | \, |w_0|^2 + |w_1|^2 = 1\}$$

of the space $\mathbf{R}^4$ by the prescription

$$\lambda \cdot (w_0, w_1) = (\lambda . w_0, \lambda . w_1).$$

In this context, the two–sphere $\mathbf{S}_2 \hookrightarrow \mathbf{R}^3$ is considered as the union of two copies $\{\mathbf{C}_0, \mathbf{C}_1\}$ of the complex plane $\mathbf{C}$ equipped with opposite orientations. The identification is performed by

$$\mathbf{S}_2 = \mathbf{C}_0 \cup_\varphi \mathbf{C}_1$$

where the assignment $\varphi : \mathbf{C}_0^\star \longrightarrow \mathbf{C}_1^\star$ of the multiplicative groups is defined by the orientation reversing map

$$\varphi(z_0) = z_1 = z_0^{-1}.$$

The complex planes $\{\mathbf{C}_0, \mathbf{C}_1\}$ are identified with planar coadjoint orbits of G (*ordo orbium*) and arranged so that the positive real axes of their symplectic structures are parallel. The positive real axes are assumed to be logarithmically scaled. Then this scaling is compatible with the opposite orientations of $\{\mathbf{C}_0, \mathbf{C}_1\}$.

The map φ may be regarded as arising from two stereographic projections from the antipodal points of the sphere $\mathbf{S}_1$. The sphere $\mathbf{S}_1$ is arranged so that it is tangential to the real axes of the sandwich configuration. The projection $\pi : \mathbf{S}_3 \longrightarrow \mathbf{S}_2$ is given by

$$\pi : w \rightsquigarrow \begin{cases} \frac{w_1}{w_0} \in \mathbf{C}_1 & \text{if} \quad w_0 \neq 0 \\ \frac{w_0}{w_1} \in \mathbf{C}_0 & \text{if} \quad w_1 \neq 0 \end{cases}$$

Notice that if $w_0.w_1 \neq 0$, the two definitions agree. It is easy to verify that $\pi(u) = \pi(v)$ for $u, v \in \mathbf{S}_3$ if and only if $u = \lambda.v$ holds for some $\lambda \in \mathbf{T}$. The trivializations are

$$\pi^{-1}(\mathbf{C}_0) = \mathbf{C}_0 \times \mathbf{T}$$

$$(w_0, w_1) \rightsquigarrow \left(\frac{w_1}{w_0}, \frac{w_0}{|w_0|}\right),$$

and

$$\pi^{-1}(\mathbf{C}_1) = \mathbf{C}_1 \times \mathbf{T}$$

$$(w_0, w_1) \rightsquigarrow \left(\frac{w_0}{w_1}, \frac{w_1}{|w_1|}\right),$$

and the chart change between these is seen to be

$$\mathbf{C}_0^\star \times \mathbf{T} \longrightarrow \mathbf{C}_1^\star \times \mathbf{T}$$

$$(z, \lambda) \rightsquigarrow \left(\frac{1}{z}, \frac{\lambda.z}{|z|}\right).$$

Since the chart change is of the form $(z, \lambda) \rightsquigarrow (\varphi(z), h(z).\lambda)$, it defines a $\mathbf{T}$ bundle over the two–sphere $\mathbf{S}_2 \hookrightarrow \mathbf{R}^3$. The inverse image of a circle on $\mathbf{S}_2$ in $\mathbf{S}_3$ is a torus. Picturing $\mathbf{S}_3 \hookrightarrow \mathbf{R}^4$ minus the north pole of $\mathbf{R}^3$ via stereographic projection provides the fibers corresponding to the places where the ratio $\frac{w_1}{w_0}$ is constant. The subset of $\mathbf{R}^3$ consisting of $\{\mathbf{R}^3 - \{z - \text{axis}\} - \{\text{central circle}\}\}$ is foliated by the tori lying over the lines of latitude on the two–sphere $\mathbf{S}_2$.

3 The Hopf fibration

All but two fibers of the Hopf bundle are located on the previously described tori in the space $\mathbf{R}^3$. On each torus the fibers run around once in each direction. The base $\mathbf{S}_2 \hookrightarrow \mathbf{R}^3$ may be regarded as the space of fibers in the sense that the projection

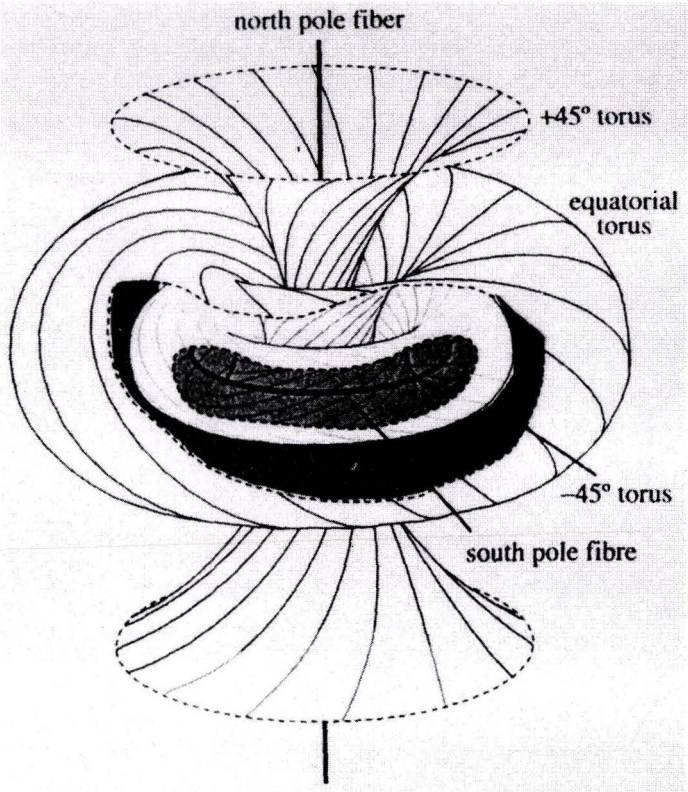

Fig. 1: Visualization of the Hopf fibration $\mathbf{S}_1 \longrightarrow \mathbf{S}_3 \longrightarrow \mathbf{S}_2$.

$\pi : \mathbf{S}_3 \longrightarrow \mathbf{S}_2$ establishes a bijection between the set of fibers and the base. Moreover, the topology on the base indicates the mutual disposition of the fibers in the sense that two fibers are "near" each other when the corresponding base points are near each other. The space of fibers of the Hopf bundle fits together topologically to form the unit two–sphere $\mathbf{S}_2$. Indeed, if one of the tori has been singled out, a cross–sectional disc for the corresponding solid torus meets every fiber inside the torus just once. The complimentary disc meets each fiber outside the torus once. Finally, the fibers on the torus meet each disc once in its bounding circle and provide a diffeomorphism between these two circles. Thus the space of fibers is made up of two 2–discs glued together by a diffeomorphism of their boundaries, which is just the unit two–sphere $\mathbf{S}_2$.

4 The minimal loop group model

The Heisenberg nilpotent Lie group G that is relevant for the imaging process of clinical magnetic resonance tomography arises from the central extension of the group $\mathrm{Loop}(\mathbf{T})$ of smooth loops of the torus group ([4]). It follows

$$\mathrm{Loop}(\mathbf{T}) = \hat{\mathbf{T}} \times \mathbf{T} \times V$$

where

$$\hat{\mathbf{T}} = \mathrm{Hom}(\mathbf{T}, \mathbf{T}) = \mathbf{Z}$$

is the discrete dual group of $\mathbf{T}$, and V denotes the real vector space of smooth maps

$$\Phi : \mathbf{S}_1 \longrightarrow \mathrm{Lie}(\mathbf{T})$$

of integral 0. Due to the sandwich configuration with logarithmically scaled positive real axes, the restriction

$$\Phi|\mathbf{S}_0$$

of Φ to $\mathbf{S}_0 \hookrightarrow \mathbf{S}_1$ provides an embedding of the three–dimensional Heisenberg group G into the Heisenberg group associated to the real vector space V. The antipodal map $\Phi|\mathbf{S}_0$ which is defined on the set

$$\mathbf{S}_0 = \{\text{spin up}\,,\ \text{spin down}\}$$

has its natural origin in the spinor approach to celestial mechanics ([1], [2], [8]).

Due to the coadjoint orbit picture of G, the unitary dual of the neutral component

$$\mathrm{Loop}(\mathbf{T})^\circ = \mathbf{T} \times G$$

of $\mathrm{Loop}(\mathbf{T})$ is then a stack of affine planes in $\mathbf{R}^3$, augmented by the singular plane of single point orbits of G. The flatness of the coadjoint orbits implies the square integrability modulo center of the associated irreducible unitary linear representations of G. As a consequence, the affine planes of the stack are appropriate substrates of image data storage ([6]).

5 Single–section acquisitions

For single–section imaging techniques of magnetic resonance tomography, the acquisition time of an image is directly proportional to the repetition time $\mathrm{T_R}$. When a single image is created using one repetition for each value of the phase–encoding gradient, the image acquisition time is the number of phase–encoding steps times $\mathrm{T_R}$. Therefore, single–section acquisitions usual have short repetition times, typically 50

msec or less. If a short T_R is acceptable or desirable, single–section acquisitions may be appropriate. Image acquisition of one section does not begin until acquisition and data organization of the previous section is complete.

For some diagnostic applications, short image acquisition time is considered paramount. In such situations, T_R is chosen as the minimum interval achievable within the constraints of the pulse train and hardware. The repetion time is defined by the echo time T_E and the time required for application of the radiofrequency pulse trains and image gradients. For rapid imaging techniques, minimizing T_R, and thus acquisition time, requires the use of the shortest possible T_E.

6 Multisection acquisitions

For many applications of clinical magnetic resonance imaging, longer repetition times T_R is desirable or essential, for example, to increase the signal intensity of tissues that have long T_1 relaxation times. For images with long T_R, single–section acquisition techniques are unacceptable inefficient, since the time between measurement of the response and the next excitation radiofrequency pulse is idle. Rather than waste the time during the interval between the T_E and the next excitation pulse, a different section can be excited by reapplying an excitation pulse of slightly different carrier frequency so that it corresponds to the frequency of a different location along the linear section–select gradient. This results in excitation of a second section, which is followed by measurement of the spin response from this second section at its echo time T_E. If time permits, additional sections can be thus excited in an interleaved manner during each T_R, followed each time by measurement of the resulting spin response. Typically, the sections are not excited exactly in sequential order but in such a way as to maximize the time elapsing between excitation of adjacent sections to reeduce the effects of cross–talk.

As an example, let $T_R = 40$ msec and $T_E = 5$ msec. Section # 1 is first excited by a radiofrequency pulse, during application of the section–select gradient, and a spin response is sampled whose peak follows 5 msec after the excitation pulse. Next, the section–select gradient is reapplied along with an excitation pulse with a slightly different carrier frequency that matches the frequency of section # 3, In practice, however, an exciation pulse cannot occur immediately after each response peak, because time is required to finish sampling the spin response and to apply additional spoiling and crushing gradients to reduce image artifacts. In this example, let the time delay be 5 msec between each response peak and the next excitation pulse. Thus, section # 3 is excited 10 msec after section # 1. Next in order, the carrier frequency of the excitation pulse is changed so that sections # 2 and # 4 are excited, generating their respective responses 5 msec after excitation pulse. Finally, at the T_R, 40 msec after the initial excitation pulse, the value of the phase–encoding

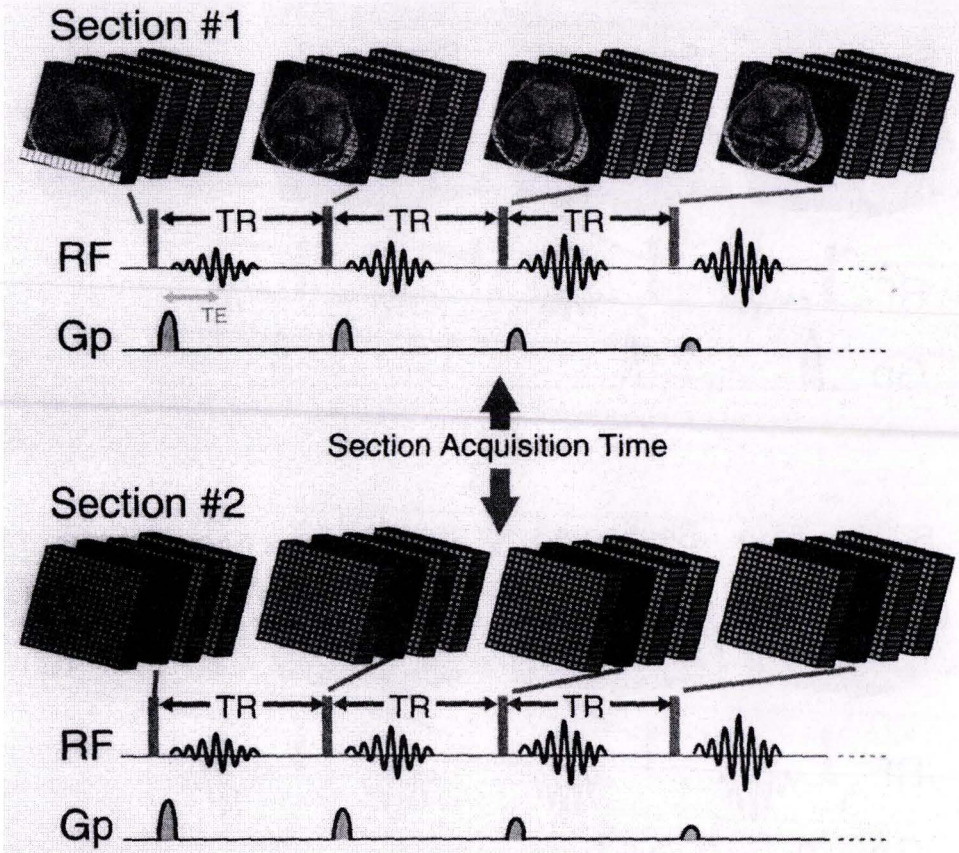

Fig. 2: Train of radiofrequency (RF) pulses and phase–encoding gradients (Gp) involved in imaging a stack of sections using single–section acquisition. A given section is excited repeatedly, varying the strength of the phase–encoding gradient. As the phase–encoding gradient strength decreases, the magnitude of the response amplitude increases. After enough responses have been received to complete acquisition of a given section, the procedure is repeated for a different section.

gradient is changed and section # 1 receives its second excitation pulse from the train.

7 Volume acquisition

Alternatively, it is possible to construct a three–dimensional image using a single frequency–encoding gradient for one in–plane axis and phase encoding for the two

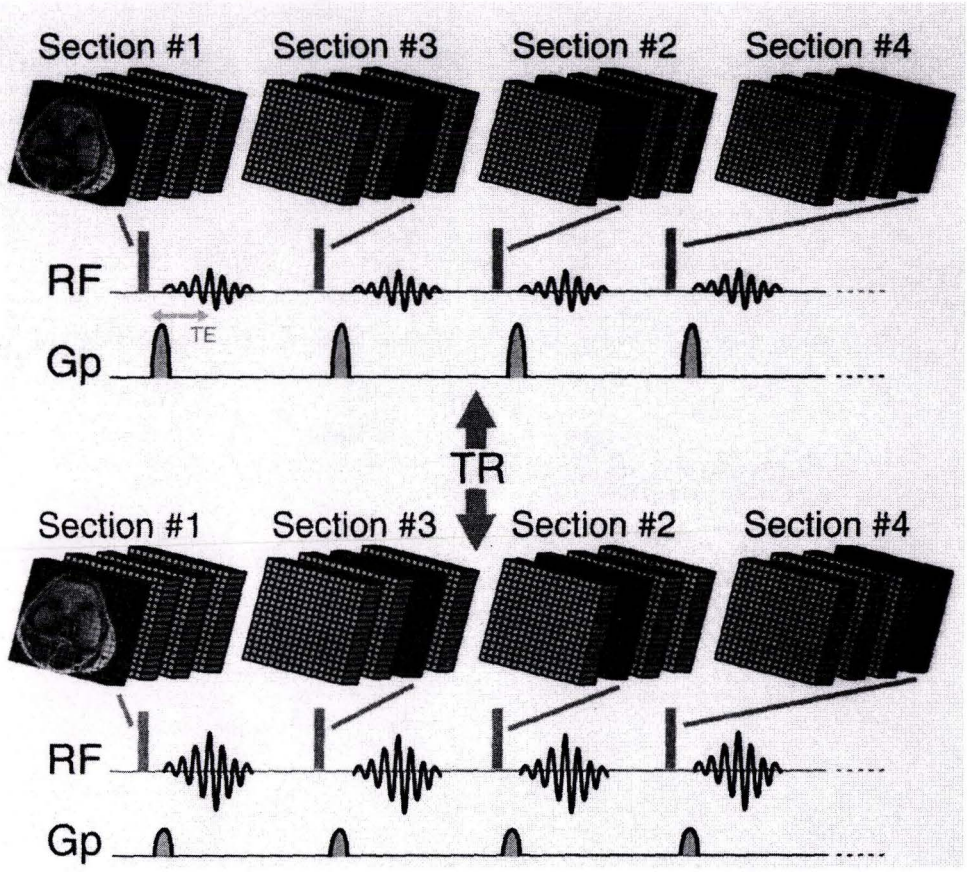

Fig. 3: Train of radiofrequency (RF) pulses and phase–encoding gradients (Gp) involved in imaging a stack of sections using multisection acquisition. Each section is excited using a given strength of the phase–encoding gradient. After each section has been excited once, all sections are excited a second time, using a different phase–encoding gradient.

other axes. This procedure, whereby multiple signals are acquired using different values of phase–encoding gradients along two different axes, is termed volume acquisition. This is similar to the description of two–dimensional imaging, except that two–dimensional sections may be separated by gaps whereas three–dimensional section form contiguous Cavalieri partitions ([6]). With two–dimensional imaging, the excitation pulse is targeted to single image section by the section–select gradient, and each resulting spin response contains signals throughout that single section. With three-dimensional imaging, however, each excitation pulse excites the entire volume, and each resulting echo contains signals from throughout the entire volume. Due to the third Kepplerian law, three–dimensional techniques generate images with

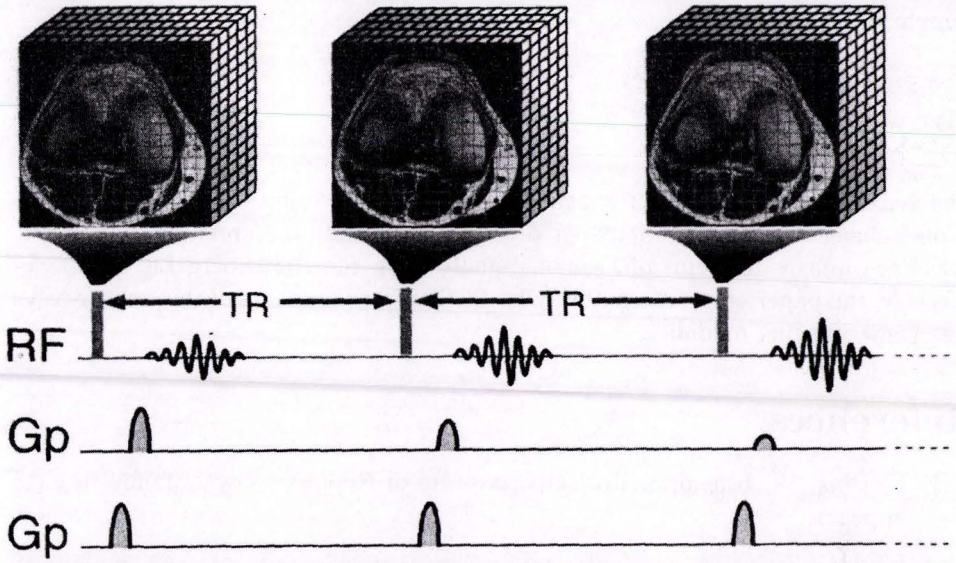

Fig. 4: Protocol of volume acquisition. The entire volume is excited by each excitation pulse. Phase encoding (Gp) is performed by linear gradients in two orthogonal directions.

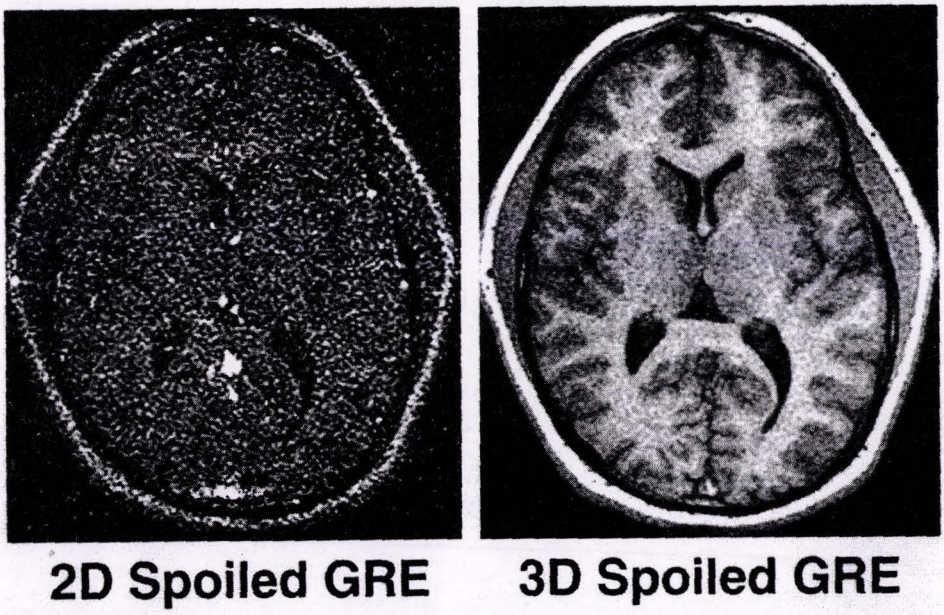

Fig. 5: Transversal cranial magnetic resonance imaging: Two–dimensional acquisition versus volume acquisition. The signal–to–noise ratio is much better with the three–dimensional technique.

much higher signal–to–noise ratio than do two–dimensional single–section images of comparable voxel size.

8 Conclusion

The sensitivity of magnetic resonance imaging for detection of soft-tissue lesions is unchallenged. The present paper describes rigorously the creation of magnetic resonance images in terms of harmonic analysis on the Heisenberg Lie group. In this way, the paper opens the pathway for further improvements of this non-invasive diagnostic imaging modality.

References

[1] E. Binz, W. Schempp, Projective aspects of Keppler's laws. Manuscript (to appear)

[2] E. Binz, W.J. Schempp, Die Kepplerschen Resonanzstrategien aus heutiger Sicht (to appear)

[3] D.G. Mitchell, MRI Principles. W.B. Saunders, Philadelphia, London, Toronto 1999

[4] A. Pressley, G. Segal, Loop Groups. Oxford University Press, Oxford, New York, London 1990

[5] W. Schempp, Harmonic Analysis on the Heisenberg Nilpotent Lie Group, with Applications to Signal Theory. Pitman Research Notes in Mathematics Series, Vol. 147, Longman Scientific and Technical, London 1986

[6] W.J. Schempp, Magnetic Resonance Imaging: Mathematical Foundations and Applications. Wiley–Liss, New York, Chichester, Weinheim 1998

[7] W. Schempp, Sub–Riemannian geometry and clinical magnetic resonance tomography. Math. Meth. Appl. Sci. 22, 867–922 (1999)

[8] E.L. Stiefel, G. Scheifele, Linear and Regular Celestial Mechanics. Springer–Verlag, Berlin, Heidelberg, New York 1971